$ReaxFF_{MgH}$ Reactive Force Field for Magnesium Hydride Systems

Sam Cheung, Wei-Qiao Deng, Adri C. T. van Duin, and William A. Goddard III*

Materials and Process Simulation Center, Division of Chemistry and Chemical Engineering, California Institute of Technology, Pasadena, California 91125

Received: September 3, 2004; In Final Form: November 5, 2004

We have developed a reactive force field ($ReaxFF_{MgH}$) for magnesium and magnesium hydride systems. The parameters for this force field were derived from fitting to quantum chemical (QM) data on magnesium clusters and on the equations of states for condensed phases of magnesium metal and magnesium hydride crystal. The force field reproduces the QM-derived cell parameters, density, and the equations of state for various pure Mg and MgH_2 crystal phases as well as and bond dissociation, angle bending, charge distribution, and reaction energy data for small magnesium hydride clusters. To demonstrate one application of $ReaxFF_{MgH}$, we have carried out MD simulations on the hydrogen absorption/desorption process in magnesium hydrides, focusing particularly on the size effect of MgH_2 nanoparticles on H_2 desorption kinetics. Our results show a clear relationship between grain size and heat of formation of MgH_2; as the particle size decreases, the heat of formation increases. Between 0.6 and 2.0 nm, the heat of formation ranges from −16 to −19 kcal/Mg and diverges toward that of the bulk value (−20.00 kcal/Mg) as the particle diameter increases beyond 2 nm. Therefore, it is not surprising to find that Mg nanoparticles formed by ball milling (20−100 nm) do not exhibit any significant change in thermochemical properties.

1. Introduction

Metal hydrides such as, LiH, CaH_2, and MgH_2 have widely been studied for hydrogen storage capabilities, and among them, MgH_2 has been widely studied because of its comparatively weaker M−H bonding.[1,2] However, the slow sorption kinetics characteristics for Mg-based materials have so far hampered commercial usage. An important reason for the slow kinetics of H desorption/adsorption is the high enthalpy of formation of the metal hydride (−17.88 kcal/mol),[3] indicating that hydrogen atoms bind too strongly with the Mg atoms. Consequently, dehydrogenation of magnesium hydrides requires high temperature (∼552 K at 1 atm). Hence, it is necessary to decrease the desorption temperature to obtain a suitable hydrogen storage material. Numerous methods have been focused on improving the problematic sorption kinetic, including mechanical ball milling[4,5,6] and mechanical alloying.[7,8] However, these methods can only improve adsorption and not desorption kinetics,[9] possibly because even the smallest particle sizes obtainable by these methods (20 nm) still primarily display bulk desorption characteristics. To determine whether a further reduction of particle size could sufficiently destabilize the MgH_2 nanoparticles and thereby lowering the hydrogen desorption temperature to values workable for mobile applications (100 °C), we have developed a reactive force field for magnesium and magnesium hydrides ($ReaxFF_{MgH}$). Although quantum chemical (QM) and semiempirical methods can be applied to study reactivity in metal hydride systems,[10,11] the computational expense of these methods severely hampers application to large (≫100 atoms) high-temperature dynamical systems. Earlier on, we have demonstrated that the ReaxFF potential can accurately describe reactive processes, including the relative stability of reactive substrates and products as well as high-energy transition states and reaction intermediates, for a wide range of chemical systems, including hydrocarbons,[12] nitramines,[13] silicon/silicon oxides,[14] and aluminum/aluminum oxides.[15] This paper presents the new force field that aims for accurate and consistent predictions of covalent systems (Mg_nH_{2n}) and all phases of magnesium hydride (including high-energy diamond and fluorite MgH_2 phases). The remainder of this paper is organized as follows: Section 2 describes the development for the Mg/MgH reactive force field and theoretical approach. The results and applications are given in section 3. Section 4 presents our discussion, and concluding remarks are given in section 5.

2. $ReaxFF_{MgH}$ Reactive Force Field for Mg and MgH_2

The development strategies for $ReaxFF_{MgH}$ are in line with those used in generating the reactive force field for hydrocarbons,[12] Si/SiO_2,[14] and $Al/\alpha\text{-}Al_2O_3$[15] systems. The potential functions in $ReaxFF_{MgH}$ are the same as those in $ReaxFF_{SiO}$, with the addition of one energy contribution (E_{MgH}) to distinguish the Mg−H binding energy in MgH and MgH_2 (see section 2.1). A key to the reactive force field is the formalism that allows for accurate description of bond formation and bond breaking by means of a bond order/bond distance relationship similar to that incorporated in the Tersoff,[16] Brenner,[17] and EDIP[18] potentials and charge transfer. ReaxFF incorporates the EEM charge calculation method[19] which allows for a polarizable, geometry-dependent charge distribution. By calculating nonbonded van der Waals and Coulomb interactions between all atoms (including 1−2 and 1−3 interactions), ReaxFF can be applied to both covalent and ionic systems.

In ReaxFF, the total energy expression for Mg and MgH_2 ReaxFF is divided into contributions as follows:

$$E_{sys} = E_{bond} + E_{over} + E_{under} + E_{val} + E_{MgH} + E_{vdWaals} + E_{Coulomb} \quad (1)$$

The parameters in these energy expressions were obtained from fitting to QM derived equations of state (EOS) of pure Mg and

10.1021/jp0460184 CCC: $30.25
Published on Web 01/13/2005

MgH_2 condensed phases and to reaction energies, bond dissociation profiles, and angle distortions derived from QM calculations on small finite clusters. In the hydrogenation−dehydrogenation process, it is conceivable for (i) the magnesium atom in pure magnesium metal to undergo coordination number change, (ii) phase transformation in both pure Mg and MgH_2 to occur, or (iii) the coexistence of multiple MgH_2 phases. To ensure that $ReaxFF_{MgH}$ can describe variations in coordination for pure Mg, we fit to the following phases: hcp (12-coordinate), fcc (12-coordinate), bcc (8-coordinate), sc (6-coordinate), and diamond (4-coordinate). To ensure a good description for MgH_2 phases, we fit to the γ-MgH_2, β-MgH_2, ϵ-MgH_2, CaF_2-MgH_2, and diamond-MgH_2, along with the ground state α-MgH_2 structure.

To provide additional test cases for the reactive potential, DFT studies were carried out on angle bending and bond dissociation of small representative magnesium−hydrogen clusters.

The EEM parameters were optimized to reproduce Mulliken charge distributions of small Mg−H clusters calculated from DFT methods. The EEM parameters for H were determined in $ReaxFF_{CH}$, so we allowed only the parameters for Mg to vary in our optimization.

2.1. Bond Energy Function. One modification to the potential functions used in $ReaxFF_{MgH}$ is the addition of MgH undercoordination correction bond energy function (eq 2). In $ReaxFF_{CH}$, separate functional forms (BO^{σ}, BO^{π}, and $BO^{\pi\pi}$) were used to describe single, double, and triple bonds; however, only the single bond was used in determining the overall bond order in $ReaxFF_{MgH}$. Magnesium is a simple $3s^2$ metal with no d electrons and a valency of two and such prefers to make single bonds. The parameters for the BO^{σ} functional were determined from Mg−Mg and Mg−H bonds

$$E_{\mathrm{MgH}} = k_{c2}(\mathrm{BO}_{ij} - \Delta_i - 0.004\Delta_i^4 - 1)^2 \quad \text{if } \mathrm{BO}_{ij} - \Delta_i - 0.004\Delta_i^4 > 1$$

$$E_{\mathrm{MgH}} = 0 \quad \text{if } \mathrm{BO}_{ij} - \Delta_i - 0.004\Delta_i^4 \le 1 \qquad (2)$$

on small magnesium hydride clusters such as MgH, MgH_2, Mg_2H_2, Mg_2H_4, and Mg_4H_8. DFT calculations for the dissociation of the Mg−H single bond gave dissociation energies of 72 kcal/mol for breaking the first Mg−H bond in MgH_2 and 33 kcal/mol for breaking the second Mg−H bond. Dissociation of the hydrogen atom from the MgH fragment requires removal of an electron from the sigma antiorbital and leaves Mg in its most stable closed-shell configuration. Dissociation of the hydrogen atom from MgH_2 leaves an unpaired electron in the antibonding orbital, yielding an energetically less stable electronic configuration. This explains the discrepancy in the two Mg−H bond dissociation energy and the following trend for Mg−H dissociation energy:

$$D_{\mathrm{HMg-H}}(72\ \mathrm{kcal}) \ll D_{\mathrm{Mg-H}}(33\ \mathrm{kcal})$$

To properly differentiate between the two Mg−H bond dissociation energies, we have included an additional term in the ReaxFF energy expression (E_{MgH}).

2.2. Method and Force Field Optimization Procedure. *QM Calculations and Force Field Optimization.* Parameter values for the potential functions were obtained by optimization against a set of data obtained from quantum chemical methods. For nonperiodic systems, DFT calculations were performed using the Jaguar program (version 4.01) with the B3LYP functional[20] and a 6-311G**++ basis set. A smaller basis set without diffuse functions were used to obtain Mulliken charge distributions.

The plane wave code CASTEP[21] was used to perform DFT calculations on the condensed states of pure magnesium and magnesium hydride systems. The generalized gradient approximation (GGA) proposed by Perdew, Burke, and Ernzerhof[22] was used for the exchange-correlation energy and ultrasoft pseudopotentials to replace the core electrons. For both the Mg and MgH_2 crystals, we used the Perdew−Wang implementation of GGA,[23] a kinetic energy cutoff of 380 eV, and the Monkhorst−Pack scheme[24] to generate the *k*-space grid using a spacing of 0.1 $Å^{-1}$. The force field was optimized against these QM data using a successive one-parameter technique.[25] The final force field parameters can be found in Tables 5−10; an overview of all the potential functions can be obtained from the supplementary material.[26]

MD Simulations. To generate Mg and MgH_2 particle of various grain size of interest (0.6−2.2 nm), a bond order cutoff was used to generate a radial diameter (from a central Mg atom) in which spherical clusters can be cut from both the Mg (hcp) and α-MgH_2 supercell geometry using the Crystal Builder module in Cerius2.[27] The supercell geometry was constructed from quantum optimized bulk structures using GGA lattice parameters[28] when possible. The simulation procedure follows: (a) Each particle was first minimized using low-temperature MD. (b) For both the equilibration and annealing runs, we perform NVT MD simulations using the Berendsen thermostat.[29] A time step of 0.25 fs was used in all simulations. Atomic charges were updated at every MD simulations.

The minimized, equilibrated, and annealed structure for a representative $Mg_{40}H_{80}$ (1.2 nm in diameter) particle is depicted in Figure 8.

3. Results

3.1. Bond Dissociation. To optimize bond energy, DFT calculations were carried out for dissociation of single Mg−H and Mg−Mg bonds in various small clusters. Figure 1a,b shows the Mg−H bond dissociation curves in MgH and MgH_2 while Figure 1c shows the data for the dissociation of two Mg−H single bond in Mg_2H_4 to give two units of MgH_2. Figure 1d shows the Mg−Mg bond dissociation curve in Mg_2H_2. In each case, DFT calculations were carried out for both singlet and triplet systems (in the case of MgH, doublet and quartet systems), and bond parameters were optimized to the lowest energy points along the dissociation curve. For every monomer, bond restraints were applied to the internal coordinate of interest while the rest of the structure was allowed to relax during the minimization.

3.2. Valence Angle Terms. To optimize the valence angle parameters for $ReaxFF_{MgH}$, we calculated angle bend energies from DFT calculations on small clusters of magnesium hydrides. There are three relevant valence angle (Mg−H−Mg, Mg−Mg−H, Mg−H−Mg) cases for which we ran DFT calculations on representative monomers. For every monomer, angle restraints were applied to fix valence angles at various values while the rest of the structure was allowed to relax during minimization. From these DFT calculations, we obtained a valence angle curve against which the $ReaxFF_{MgH}$ parameters can be optimized. Figure 2 shows a comparison between the $ReaxFF_{MgH}$ and DFT energies as a function of the H−Mg−H valence angle. $ReaxFF_{MgH}$ and DFT data for the other two angles are given in the supplementary material.[26]

3.3. Charge Distributions. In $ReaxFF_{MgH}$, charge distributions are calculated using the EEM[19] method. Mulliken charge

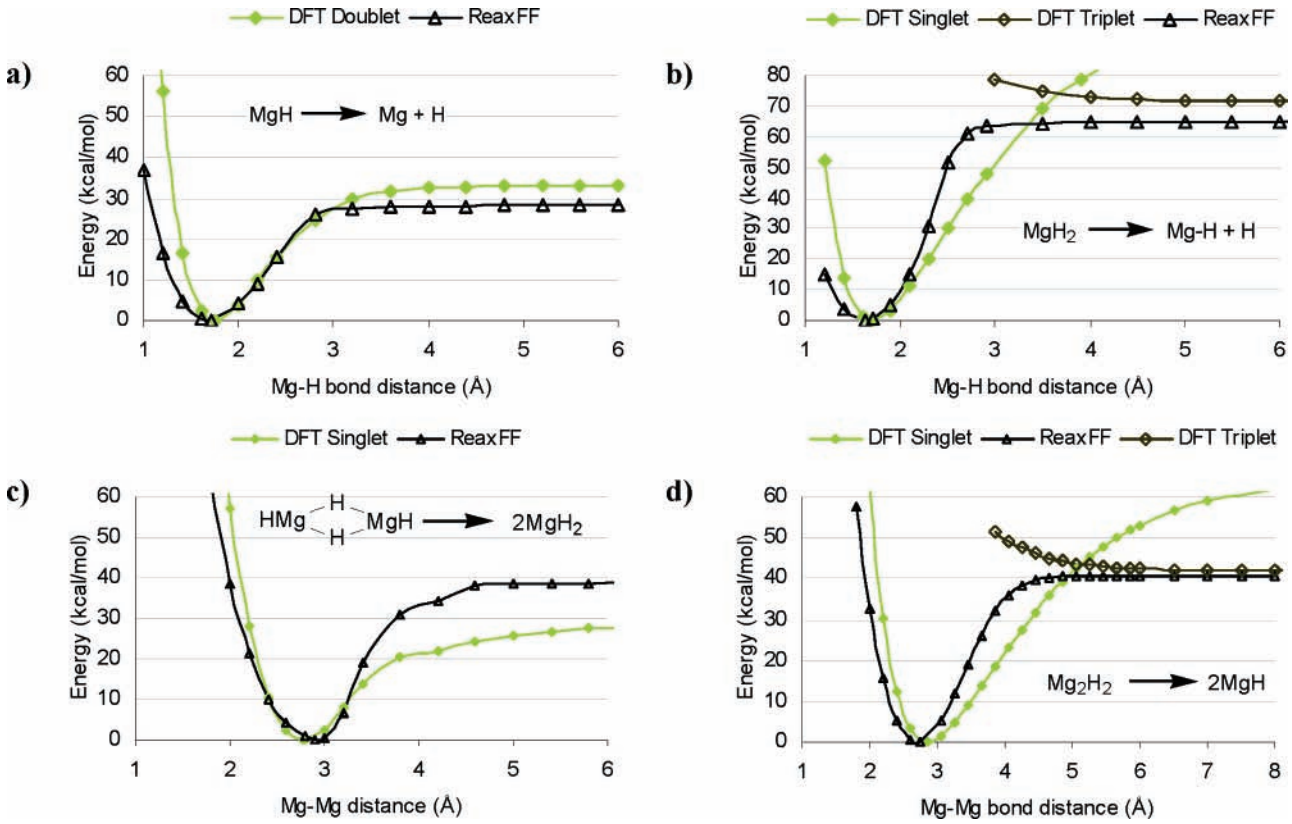

Figure 1. Bond dissociation curves for small MgH clusters as calculated by the ReaxFF and DFT methods. Dissociation of the (a) Mg−H bond in MgH, (b) Mg−H bond in MgH_2, (c) two bridging Mg−H bonds in Mg_2H_4, and (d) Mg−Mg bond in Mg_2H_2.

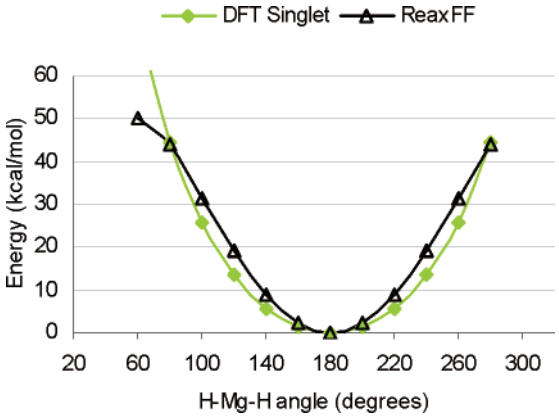

Figure 2. Energy curve of MgH_2 as a function of the H−Mg−H valence angle.

TABLE 1: Comparison between DFT and ReaxFF Reaction Energies (kcal/mol) for Magnesium Hydride Systems

reaction	E_{DFT}	E_{ReaxFF}
$MgH_2 \rightarrow {}^1/_2Mg_2H_4$	−14.3	−19.8
$MgH_2 \rightarrow {}^1/_4Mg_4H_8$	−21.5	−26.5
$Mg_2H_4 \rightarrow {}^1/_2Mg_4H_8$	−7.2	−6.7
$MgH_4 \rightarrow MgH_2 + H_2$	−87.7	−64.1
$MgH_2 + H \rightarrow MgH + H_2$	−38.0	−32.5
$MgH + H \rightarrow Mg + H_2$	−77.0	−70.1
$Mg_3H_2 \rightarrow Mg_2H + MgH$	−36.7	−25.4
$Mg_2H_2 + H_2 \rightarrow Mg_2H_4$	−17.2	−33.5
$MgH_2 + Mg \rightarrow Mg_2H_2$	−3.0	−4.4

distributions obtained from DFT calculations with the 6-31G**-basis set were used to optimize EEM parameters (Table 6). The comparison between ReaxFF and DFT data on partial charges for the Mg and H atoms in small Mg_nH_{2n} clusters are plotted in Figure 3. ReaxFF successfully reproduces charge assignments for all clusters.

3.4. Reaction Energies. To sample all possible covalent environment of the Mg−H bond, we carried out DFT and $ReaxFF_{MgH}$ calculations on the reaction energies for small Mg_nH_{2n} clusters (Figure 4). Table 1 provides a comparison between DFT and $ReaxFF_{MgH}$ results for these reactions.

3.5. Condensed Phase Data. One main objective is to apply $ReaxFF_{MgH}$ to study the magnesium particle size effect on the thermochemistry of the hydrogen absorption/desorption process. Hydrogenation of pure magnesium produces MgH_2 containing 7.6 mass % hydrogen. However, its formation from bulk magnesium and gaseous hydrogen is extremely slow and requires a temperature of 300 °C under a hydrogen pressure of 0.01 MPa. At ambient pressure and low temperatre α-MgH_2 crystallizes with the TiO_2-rutile-type structure but transforms into orthorhombic γ-MgH_2 at higher temperature and pressures. The α- to γ-MgH_2 transition pressure has not yet been experimentally determined. However, in previous theoretical work on pressure-induced transformations in MgH_2, Vajeeston and co-workers[28] found that, at equilibrium, the energy difference between α-MgH_2 and γ-MgH_2 modifications is very small and concluded that both phases can coexist under a certain field pressure. Therefore, it is important that ReaxFF be able to capture all possible modifications of MgH_2 crystals and be able to predict condensed phase stabilities. For both pure Mg and MgH_2 crystal phases, quantum energies were obtained for a wide range of compression and expansion points (Figures 5 and 6). ReaxFF correctly reproduces the structural parameters (bond distances and cell dimensions) and the equations of state for all phases of pure Mg and MgH_2 crystals. For all modifications, the cohesive energies and densities obtained from ReaxFF were compared against QC data (Tables 2 and 3). Our results are consistent with those found by Vajeeston and co-workers.[28] Furthermore, $ReaxFF_{MgH}$ calculates a heat of formation of −20.00 kcal/mol for the α-MgH_2 phase, which is in good

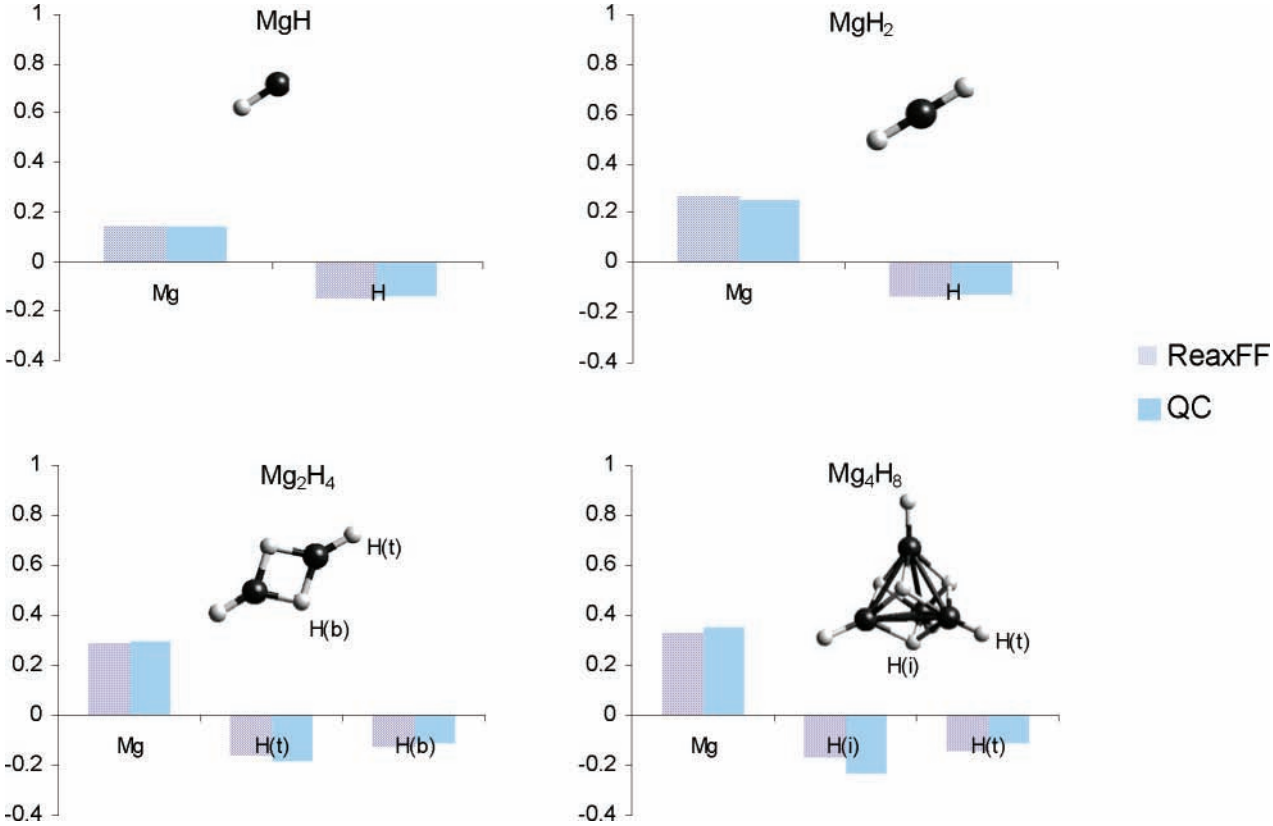

Figure 3. Comparison between Mulliken charge distributions obtained from DFT and ReaxFF charge distributions for small Mg_nH_{2n} clusters.

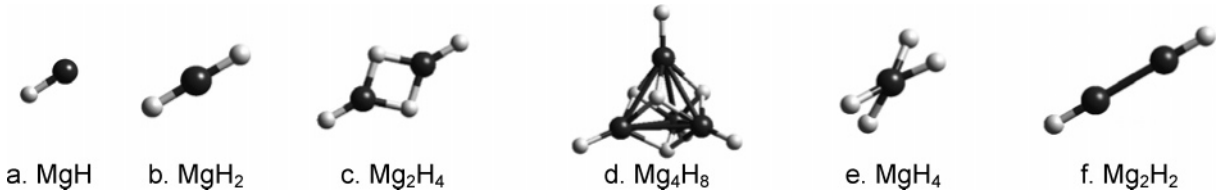

Figure 4. Mg_nH_{2n} clusters obtained from DFT simulations. Black and white balls represent Mg and H atoms, respectively.

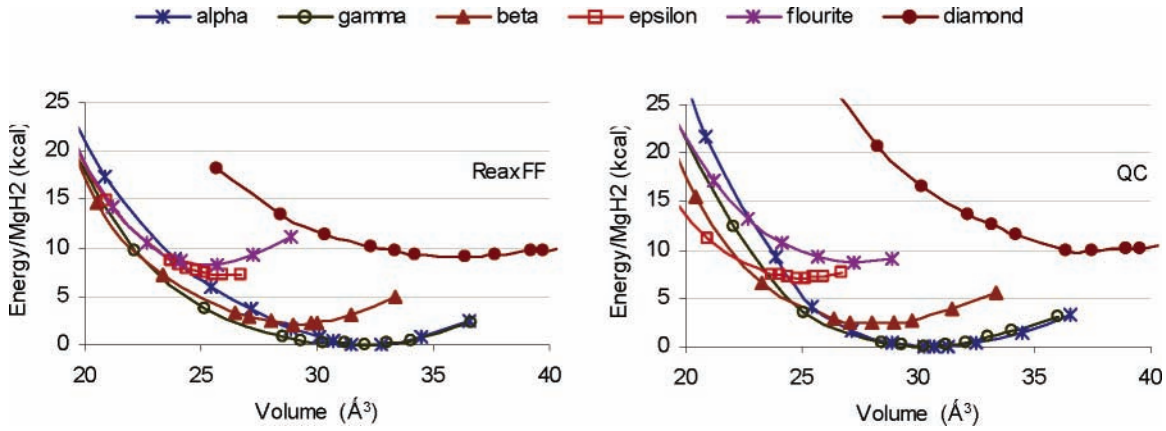

Figure 5. Equation of state (compression/expansion) for phases of magnesium as calculated by the DFT and ReaxFF methods.

agreement with QM-derived value (−16.49 kcal/mol). The DFT and $ReaxFF_{MgH}$ results for the heat of formations for other modifications of MgH_2 are compared in Table 4.

3.6. Applications. 3.6.1. Heat of Formation from Mg Particles to MgH_2 Particles. Although improvements in the kinetics of magnesium have been achieved by nanostructuring of particles down to the 20−100 nm regime, the conclusions in the changes in the thermodynamics of these particles with respect to the bulk magnesium hydride still remain open-ended.[6,9,30] To determine whether a further reduction of grain size below the 20 nm regime could sufficiently destabilize the MgH_2 nanoparticles, we have investigated the enthalpy of formation of ultrasmall MgH_2 particles below the 20 nm regime.

We carried out simulations on ultrasmall Mg and MgH_2 particles within the 0.62−2.20 nm range. Energies at 0 K for each component particle from ReaxFF annealing simulations were used to tabulate the heat of formation (Figure 7). The minimized, equilibrated, and annealed structures for one rep-

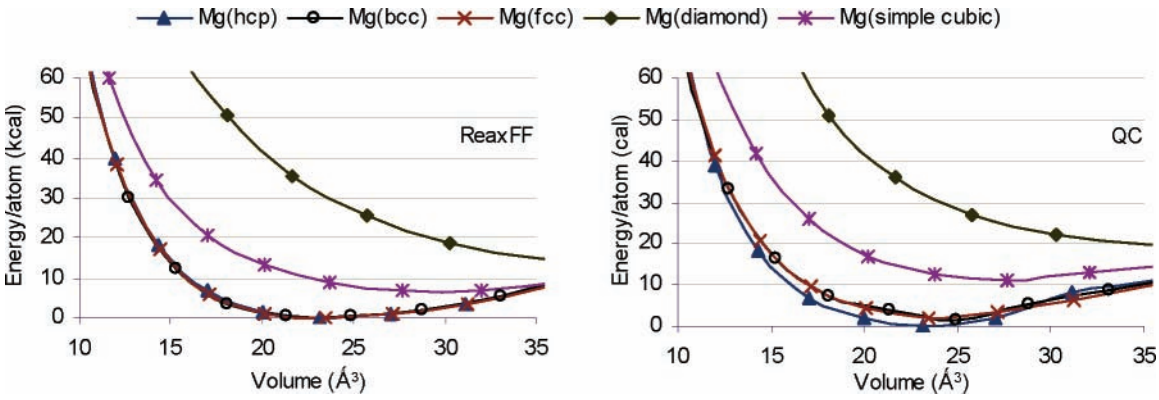

Figure 6. Equation of state (compression/expansion) for phases of magnesium hydride as calculated by the DFT and ReaxFF methods.

TABLE 2: Mg Metal Phase Stabilities (kcal/mol) Relative to Hcp

crystal phase	ΔE_{DFT}	ΔE_{ReaxFF}
fcc[a]	1.81	0.00
bcc	1.65	0.38
simple cubic	10.94	7.01
diamond	19.00	13.26

[a] ReaxFF does not distinguish between the hcp and fcc phases, and therefore the two energies are similar.

resentative $Mg_{40}H_{80}$ (1.2 nm in diameter) particle are depicted in Figure 8. The enthalpy of formation of this reaction

$$Mg_nH_{2n} \rightarrow Mg_n + nH_2 \tag{3}$$

can be written as

$$\Delta H_f = \mu_{Mg_nH_{2n}} - \mu_{Mg_n} - n\mu_{H_2} \tag{4}$$

The chemical potentials of the component systems (at $T = 0$, $P = 0$) are given as follows:

$\mu_{Mg_nH_{2n}}$ = energy per MgH_2 unit in MgH_2 nanocrystal

μ_{Mg_n} = energy per Mg unit in Mg nanocrystal

$$\mu_{H_2} = E(H_2) + \frac{1}{2}\hbar\omega_0 \tag{5}$$

In the total energy of H_2, we included zero point energy correction (ZPE = 5.33 kcal/mol; heat content = 2.37 kcal/mol). The zero-point vibrational energy corrections for the MgH_2 clusters were not included; frequency calculations are currently under development for ReaxFF. We expect the ZPE correction to improve the agreement of the heat of formation of bulk MgH_2 with DFT values. From our results, a clear trend is observed such that the heat of formation becomes more positive with decreasing grain size (Figure 10). Beyond 2 nm diameter, the heat of formation converges to the bulk value of −20.0 kcal/mol.

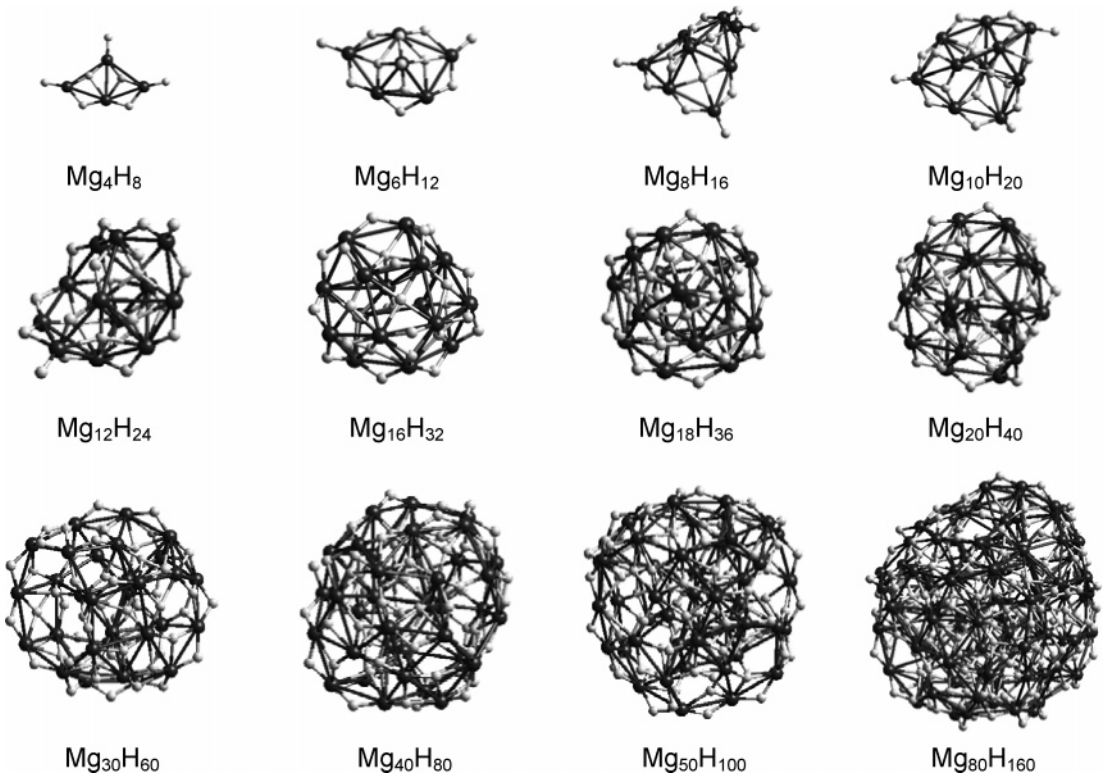

Figure 7. Final geometries of Mg_nH_{2n} particles obtained from annealing simulations using $ReaxFF_{MgH}$. Equilibrated structures (300 K) were used as starting geometries and annealed to 0 K.

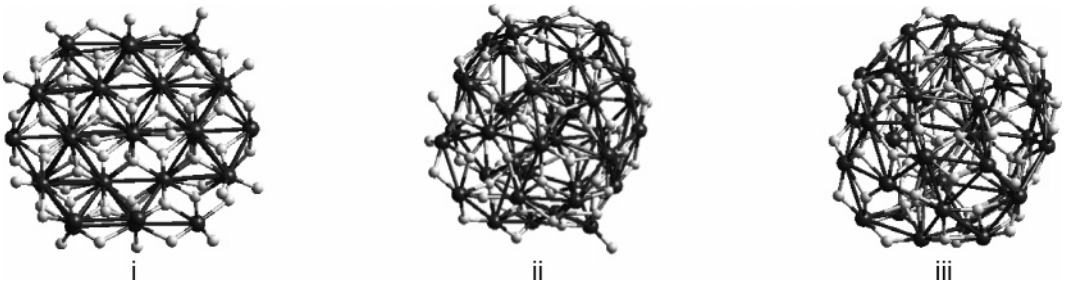

Figure 8. Geometries of $Mg_{40}H_{80}$ particle obtained from $ReaxFF_{MgH}$ simulations after (i) minimization, (ii) equilibration at 300 K for 50 000 steps, and (iii) annealing from 300 to 0 K (50 000 steps).

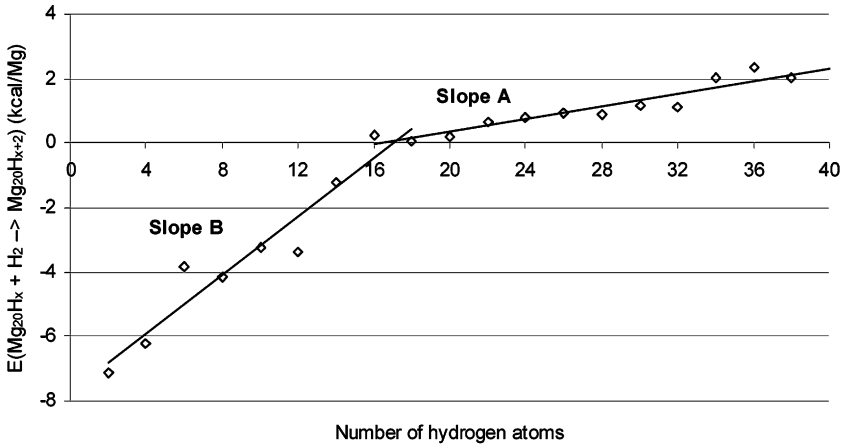

Figure 9. Energies of $Mg_{20}H_n$ particles as a function of H_2 abstraction as calculated using ReaxFF. Successive abstraction of surface H_2 were perform on $Mg_{20}H_n$ systems until all hydrogen atoms were removed. Particles were equilibrated at 300 K and annealed from 300 to 0 K before each removal of H_2. Severe depletion of surface hydrogen resulted in structures where Mg atoms preferentially occupy the surface sites; thus, the removal of hydrogen became energetically unfavorable, as evident in slope B.

TABLE 3: Condensed Phase Densities (g/cm^3)

phase	ρ_{DFT}	ρ_{ReaxFF}
Mg(diamond)	0.949	0.911
Mg(simple cubic)	1.459	1.311
Mg(bcc)	1.623	1.781
Mg(fcc)	1.721	1.760
Mg(hcp)	1.745	1.759
diamond-MgH_2	1.167	1.218
α-MgH_2	1.425	1.358
γ-MgH_2	1.445	1.383
β-MgH_2	1.561	1.514
CaF_2-MgH_2	1.604	1.578
ϵ-MgH_2	1.736	1.679

TABLE 4: Heat of Formation (kcal/MgH_2) of Various MgH_2 Phases

	DFT		ReaxFF	
phase	ΔH_{0K}	ΔH_{298K}[a]	ΔH_{0K}	ΔH_{298K}[b]
α-MgH_2	−12.04	−16.49	−12.29	−20.00
γ-MgH_2	−11.99	−16.44	−11.75	−19.45
β-MgH_2	−9.66	−14.11	−10.21	−17.91
ϵ-MgH_2	−4.91	−9.36	−3.76	−11.47
CaF_2−MgH_2	−3.04	−7.49	−3.71	−11.41
diamond-MgH_2	−2.26	−6.71	−2.81	−10.52

[a] With zero-point vibration for both α-MgH_2 and H_2 (ZPE of α-MgH_2 was used to correct for ΔH of the other MgH_2 phases.) [b] With zero-point vibration for H_2 (ZPE for MgH_2 not included, although incorporation of the ZPE for MgH_2 will raise the energy of ΔH and improve the agreement with DFT results).

3.6.2. Hydrogen Desorption. To gain better insights into the behavior of the crystal during the desorption process, we simulated the successive abstraction of surface molecular H_2 from a representative $Mg_{20}H_{40}$ nanoparticle (eq 6), where n = 38 to 0.

$$Mg_{20}H_{x+2} \rightarrow Mg_{20}H_x + H_2 \quad (6)$$

The radial distribution functions $g_{MgH}(r)$ for $Mg_{20}H_n$ systems

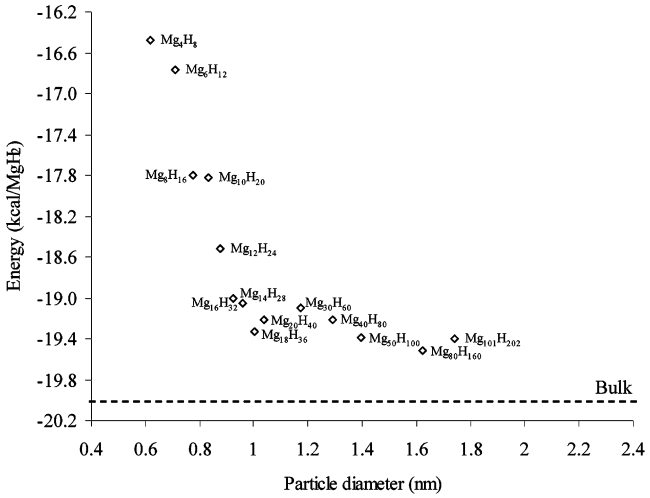

Figure 10. Variation of heat of formation of magnesium hydride particles as a function of grain size calculated using $ReaxFF_{MgH}$. The dash line represents the bulk value (−20 kcal/MgH_2).

TABLE 5: Atom Parameters

atom	$p_{ov/un}$	p_{under}	λ_{11} (val1)	$p_{v,5}$ (val3)	$p_{v,6}$ (val4)
Mg	−1.08	38.00	2.37	6.30	2.97
H	−10.00	0	2.75	6.30	2.88

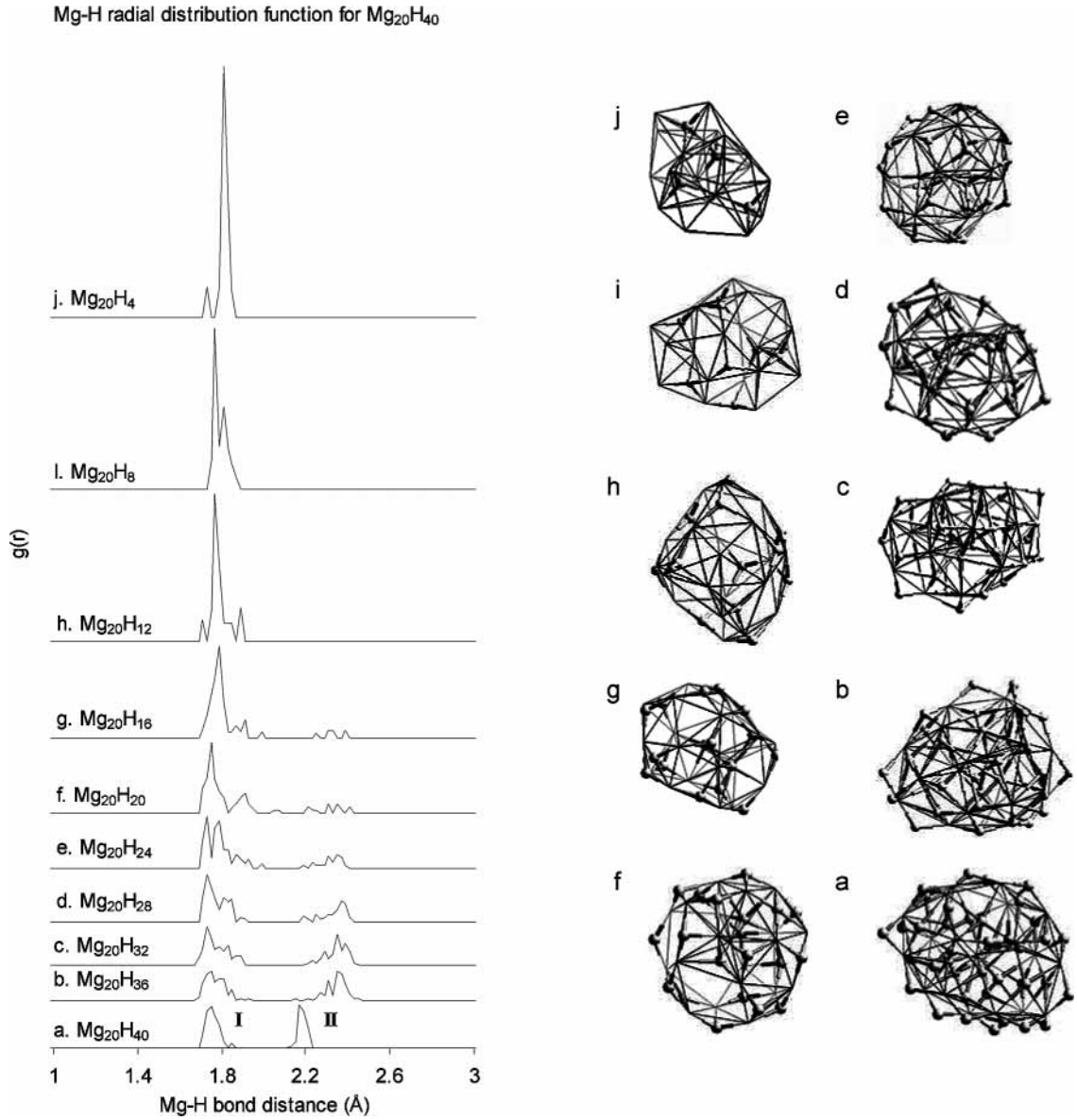

Figure 11. Mg−H radial distribution functions and structures for $Mg_{20}H_n$ systems. Lines and balls represent magnesium and hydrogen atoms, respectively. The RDF(s) calculated by Cerius[2] indicates that there are two types of hydrogen atoms (type I hydrogen atoms with an average Mg−H bond distance of 1.8 Å and type II hydrogen atoms with an average bond distance of 2.3 Å). Depletion of type II hydrogen atoms resulted in structures where Mg atoms preferentially occupy surface sites. There are no surface hydrogen atoms in the $Mg_{20}H_6$, $Mg_{20}H_4$, and $Mg_{20}H_2$ systems.

TABLE 6: Coulomb and 1−3 Bond Order Correction

	Coulomb parameters			1−3 BO correction		
atom	H (eV)	χ (eV)	γ (Å)	λ_3	λ_4	λ_5
Mg	6.00	0.52	0.40	49.9248	0.3370	0
H	9.88	3.82	0.76	4.0736	2.6883	1.00

TABLE 7: van der Waals and Bond Radius Parameters

atom	r^{σ} (Å)	r_{vdW} (Å)	ee (kcal/mol)	Aa	γ_w (Å)
Mg−Mg	1.832	4.493	0.181	10.92	27.12
Mg−H	1.294	3.200	0.010	13.29	
H−H	0.756	3.132	0.100	8.50	2.00

TABLE 8: Bond Energy Parameters (D_e^{σ} in kcal/mol)

atom	D_e^{σ}	$p_{be,1}$	$p_{be,2}$	$p_{be,3}$	E_{MgH}	p_{MgH}
Mg−Mg	32.3808	−0.0076	4.8726	0.2641		
Mg−H	58.6896	−0.0203	8.2136	0.0230	24.4461	0.0736

TABLE 9: Bond Order Parameters

bond	$p_{bo,1}$	$p_{bo,2}$
Mg−Mg	−0.0729	4.6319
Mg−H	−0.2692	6.4254

TABLE 10: Valence Angle Parameters

angle	$\theta_{0,0}$	k_a	k_b	$p_{v,1}$	$p_{v,2}$	λ_{12}
H−Mg−H	0[a]	49.8261	0.2093	0	2.0870	2.2895
H−Mg−Mg	0	8.7037	0.0827	0	3.5597	1.1198
Mg−H−Mg	0	0.5047	0.8000	0	0.8933	4.6650

[a] This value leads to an equilibrium angle of 180−0 = 180° for the single H−Mg−H valence angle.

and corresponding structures are given in Figure 11. The rdf(s) indicates two types of hydrogen corresponding to the peaks, centered at 1.7 Å (type I) and 2.3 Å (type II). Figure 9 shows a nonlinear trend in particle stability as a function of molecular hydrogen abstraction. The less strongly bound type II hydrogen atoms are first removed, resulting in the energy trend seen in slope A. Further H_2 abstraction (slope B) leads to the depletion of surface hydrogen atoms, and rearrangement produces particles

where Mg atoms preferentially occupy surface sites. Therefore, the last 14 hydrogen atoms are more strongly bound and more difficult to desorb, as evident in the steepness of slope B and the disappearance of peak II.

4. Discussion

We have generated a reactive force field for magnesium and magnesium hydride system based on the functional forms used in $ReaxFF_{SiO}$. We have shown that $ReaxFF_{MgH}$ can reproduce DFT values for the EOS, cell parameter, and density of condensed systems along with DFT geometry and reaction energies for small clusters. This overall agreement between the QC and $ReaxFF_{MgH}$ data indicates that $ReaxFF_{MgH}$ could play an important role in helping to elucidate some of the fundamental problems that hinder hydrogen absorption/desorption so that the potential of 7.6 wt % H storage capacity of magnesium can be reached. Specifically, we have used $ReaxFF_{MgH}$ to show a relationship between grain size reduction and decreased structural stability.

To demonstrate this relationship, we used MD simulations to generate Mg and MgH_2 nanoparticles and calculated their heats of formation as a function of particle size. From Figure 10, it is clear that as the nanoparticles size decreases, the heat of formation becomes more positive. In particular, there is a steep increase in the heat of formation within the ultrasmall MgH_2 particle region (0.62−0.92 nm). The decrease in structural stability of magnesium particles in this region can be attributed to two factors. First, results indicate that, below a critical particle diameter of 0.92 nm, all Mg and H atoms were exposed to the surface. It is at this region that the properties of the material begins to differ from that of the bulk properties. Second, in ultrasmall MgH_2 particles, surface hydrogen atoms are generally found to occupy the less stable top and bridge sites vs the more stable three-coordinate sites more commonly observed in larger particles. Consequently, surface Mg atoms in the ultrasmall regime are left undercoordinated. The hydrogen atoms found in these energetically less favored sites are more easily desorbed from the surface. We conclude that significant changes in the thermochemistry of hydrogen desorption is observed only if the particle grain size is reduced below 2 nm; this is in agreement with ball milling experiments which suggest that there is minor changes in the heat of formation even for the smallest particle obtainable (20 nm).[8]

To study the crystal chemistry of the magnesium hydride nanoparticles during the desorption process, we ran MD simulations on a series of $Mg_{20}H_n$ systems in which successive abstractions of surface H_2 from the system were performed. In our simulations, we did not observe any dramatic changes in atom coordination for both Mg and H, nor did we observe any major deviation in Mg−Mg and Mg−H bond lengths from the bulk values. We found that the desorption of the first half of the hydrogen atoms in the $Mg_{20}H_{40}$ system occurred with greater ease than the last half, as evident from slope A in Figure 9 and the disappearance of the type II hydrogen atoms comprising the peak centered at 2.3 Å for the RDF(s) in Figure 11. This can be attributed to the fact that for systems highly depleted in surface hydrogen atoms Mg atoms prefer to occupy surface sites. In fact, $Mg_{20}H_n$, where $n = 2$ and 4, are highly unstable structures with no surface hydrogen atoms, and abstraction of these last four hydrogen atoms would be energetically unfavorable. From slope A, we calculate a hydrogen storage capacity of 4.9 wt %, which is below its theoretical storage value of 7.6 wt %.

One concern of ultrasmall nanoparticles is rapid aggregation to form larger, more stable particles. To address this issue, we intend to investigate functionalization of the particle surface with Mg−R groups. The R groups should not hinder H_2 absorption/desorption characteristics.

In future work we aim to apply this method to investigate the kinetics of H absorption/desorption using different modifications of MgH_2 phases, the process of atomic H adsorption on the Mg (0001) surface, and the mechanistic pathway of H absorption into bulk magnesium.

5. Conclusion

By optimizing force field parameters against a substantial QM-derived training set, containing bond dissociation, angle bending, charge distribution, and reaction energy data for small clusters as well as equations of state for a range of magnesium and magnesium hydride condensed phases, we have developed a reactive force field for magnesium and magnesium hydrides ($ReaxFF_{MgH}$). $ReaxFF_{MgH}$ uses the same functional forms as previous ReaxFF descriptions, and as such, this method should be straightforwardly extendible to other magnesium-containing materials.

We have used $ReaxFF_{MgH}$ to investigate the trend in thermodynamic destabilization of magnesium hydride particles with grain size. Results indicate a steep increase in heat of formation and decrease in structural stability as particle size drop below 1.0 nm. This finding agrees with ball milling experiments that suggest that there is little change in the heat of formation even when particle size is reduced to the 20−100 nm regime; our results suggest that the particle size has to be reduced substantially below the 20 nm range to see a significant drop in particle stability.

We believe that these reactive force field methods can provide a useful computational tool to study the chemistry at surfaces and interfaces and as such could play a pivotal role in designing improved hydrogen storage materials.

References and Notes

(1) Schlapbach, L.; Züttel, A. *Nature (London)* **2001**, *414*, 353.
(2) Noritake, T.; Aoki, M.; Towata, S.; Seno, Y.; Hirose, Y.; Nishibori, E.; Takata, M.; Sakata, M. *Appl. Phys. Lett.* **2002**, *81*, 2008.
(3) Stampfer, J. F.; Holley Jr., C. E.; Suttle, J. F. *J. Am. Chem. Soc.* **1960**, *82*, 3504.
(4) Zaluska, A.; Zaluski, L.; Ström-Olsen, J. O. *Appl. Phys. A: Mater. Sci. Process.* **2001**, *72*, 157.
(5) Orimo, S.; Fujii, H.; Ikeda, K. *Acta Mater.* **1997**, *45*, 331.
(6) Zaluska, A.; Zaluski, L.; Strom-Olsen, J. O. *J. Alloys Compd.* **1999**, *288*, 217.
(7) Huot, J.; Liang; G.; Schultz, R. *Appl. Phys. A: Mater. Sci. Process.* **2001**, *72*, 187.
(8) Huot, J.; Pelletier, J. F.; Lurio, L. B.; Sutton, M.; Schulz, R. *J. Alloys Compd.* **2003**, *348*, 319.
(9) Liang, G.; Huot, J.; Boily, S.; Neste, A. V.; Schulz, R. *J. Alloys Compd.* **1999**, *292*, 247.
(10) Vegge, T. *Phys. Rev. B* **2004**, *70*, 35412.
(11) Jacobsen, K. W.; Stoltze, P.; Nørskov, J. K. *Surf. Sci.* **1996**, *366*, 394.
(12) van Duin, A. C. T.; Dasgupta, S.; Lorant, F.; Goddard, W. A. *Phys. Rev. Lett.* **2003**, *91*, 098301.
(13) Strachan, A.; van Duin, A. C. T.; Chakraborty, D.; Dasgupta, S.; Goddard, W. A. *J. Phys. Chem. A* **2001**, *105*, 9396.
(14) van Duin, A. C. T.; Strachan, A.; Stewman, S.; Zhang, Q.; Xu, X.; Goddard, W. A. *J. Phys. Chem. A* **2003**, *105*, 3803.
(15) Zhang, Q.; Çağin, T.; van Duin, A. C. T.; Goddard, W. A. *Phys. Rev. B* **2004**, *69*, 45423.
(16) Tersoff, J. *Phys. Rev.* **1988**, *61*, 2879.
(17) Brenner, D. W. *Phys. Rev. B* **1990**, *42*, 9458.
(18) Bazant, M. Z.; Kaxiras, E. *Phys. Rev. Lett.* **1996**, *77*, 4370.
(19) Mortier, W. J.; Ghosh, S. K.; Shankar, S. *J. Am. Chem. Soc.* **1998**, *120*, 2641.
(20) Becke, A. D. *J. Chem. Phys.* **1993**, *98*, 5648.
(21) Payne, M. C.; Teter, M. P.; Allan, D. C.; Arias, T. A.; Joannopoulos, J. D. *Rev. Mod. Phys.* **1992**, *64*, 1045.

(22) Perdew, J. P.; Burke, K.; Ernzerhof, M. *Phys. Rev. Lett.* **1996**, *77*, 3865.
(23) Perdew, J. P.; Wang, Y. *Phys. Rev. B* **1992**, *46*, 6671.
(24) Monkhorst, H. J.; Pack, J. D. *Phys. Rev. B* **1976**, *13*, 5188.
(25) van Duin, A. C. T.; Bass, J. M.; van de Graaf, B. *J. Chem. Soc., Faraday Trans.* **1994**, *90*, 2881.
(26) See our website http://www.wag.caltech.edu/publications/papers/.
(27) Cerius^2 package (http://www.accelrys.com).
(28) Vajeeston, P.; Ravindran, P.; Kjekshus, A.; Fjellvåg, H. *Phys. Rev. Lett.* **2002**, *89*, 175506.
(29) Berendsen, H. J. C.; Postma, J. P. M.; Van Gunsteren, W. F.; Dinola, A.; Haak, J. R. *J. Chem. Phys.* **1984**, *81*, 3684.
(30) Hanada, N.; Ichikawa, T.; Orimo, S.; Fujii, H. *J. Alloys Compd.* ***2004***, *366*, 269.